NASA Technical Memorandum 106637

A Full Navier-Stokes Analysis of Subsonic Diffuser of a Bifurcated 70/30 Supersonic Inlet for High Speed Civil Transport Application

Kamlesh Kapoor, Bernhard H. Anderson,
and Robert J. Shaw
Lewis Research Center
Cleveland, Ohio

July 1994

National Aeronautics and
Space Administration

A FULL NAVIER-STOKES ANALYSIS OF SUBSONIC DIFFUSER OF A BIFURCATED 70/30 SUPERSONIC INLET FOR HIGH SPEED CIVIL TRANSPORT APPLICATION

Kamlesh Kapoor, Bernhard H. Anderson, and Robert J. Shaw
National Aeronautics and Space Administration
Lewis Research Center
Cleveland, Ohio 44135

SUMMARY

A full Navier-Stokes analysis was performed to evaluate the performance of the subsonic diffuser of a NASA Lewis Research Center 70/30 mixed-compression bifurcated supersonic inlet for high speed civil transport application. The PARC3D code was used in the present study. The computations were also performed when approximately 2.5 percent of the engine mass flow was allowed to bypass through the engine bypass doors. The computational results were compared with the available experimental data which consisted of detailed Mach number and total pressure distributions along the entire length of the subsonic diffuser. The total pressure recovery, flow distortion, and crossflow velocity at the engine face were also calculated. The computed surface ramp and cowl pressure distributions were compared with experiments. Overall, the computational results compared well with experimental data. The present CFD analysis demonstrated that the bypass flow improves the total pressure recovery and lessens flow distortions at the engine face.

INTRODUCTION

A highly efficient propulsion system will play a critical role in the development of an economically viable and environmentally acceptable High Speed Civil Transport (HSCT). The inlet system of a supersonic cruise aircraft requires maximum total pressure recovery and minimum flow distortion at the compressor face. The drag associated with the inlet system, which primarily consists of boundary layer and cowl bleed, spillage, and bypass flow, should be minimized. The overall length of the inlet system should be shorter, consequently reducing weight. Finally, the propulsion system has to be well integrated with the airframe. These requirements have led inlet designers to consider two-dimensional, mixed-compression bifurcated inlet systems for the next-generation supersonic transport. The overall length of the bifurcated inlet is approximately one-half a single duct inlet, both supplying the same total airflow to the engine.

Bifurcated two-dimensional supersonic inlets have not been studied as extensively as axisymmetric inlets, and therefore very little is known about the aerodynamic performance of such systems. J.F. Wasserbauer, E.T. Meleason, and P.L. Burstadt experimentally studied a Mach-2.7 two-dimensional, mixed-compression bifurcated inlet with 30 percent internal contraction (NASA Lewis Research Center, Cleveland, Ohio, 1970's, unpublished data.). The inlet geometry is shown in figure 1. The flow symmetry was excellent between the separate halves of the inlet, and twin-duct instability was not observed.

The aerodynamic performance of the subsonic diffuser of the inlet just described is very critical to the overall performance of the inlet system. The objective of the present study was to perform a full Navier-Stokes analysis of the subsonic diffuser of the bifurcated inlet and to compare the numerical results with the experimental data of Wasserbauer, Meleason, and Burstadt.

The subsonic diffuser of the bifurcated supersonic inlet shown in figure 2 is a diffusing transition S-duct, which changes the cross-sectional area from a rectangle to nearly a semicircle. The overall length of the diffuser is an L/D_i of approximately 2.25, but the actual transition is achieved in an L/D_i of approximately 1.83.

The PARC3D code, which solves the full Navier-Stokes equation, was used in the present study. In the past, three-dimensional viscous subsonic flows in complex inlet duct geometries have been investigated by Briley and McDonald (refs. 1 and 2) and by Anderson (ref. 3) using Reduced Navier-Stokes equations. Harloff, Reichert, and Wellborn (ref. 4) and Sirbaugh and Reichert (ref. 5) have successfully used the PARC3D code to analyze diffusing S-duct and circular-to-rectangular transition ducts, respectively. Anderson, Reddy and Kapoor (ref. 6) compared the PARC3D with the RNS3D code for separating flows within a diffusing S-duct. Recently, Anderson and Kapoor (ref. 7) used both the RNS3D and PARC3D codes to conduct a parametric study of bifurcated diffusing transition S-ducts.

It is evident from the literature cited that the PARC3D code has successfully been used to predict flow fields in the complex geometry of inlet ducts.

SYMBOLS

A	area
D	inlet width
L	length
M	Mach number
m	mass flow
Pt	total pressure
p	static pressure
R	radius
R_{ef}	engine face radius
R_s	spinner fairing radius
Tt	total temperature
u_τ	friction velocity, $\sqrt{\tau_w/\rho_w}$
X	axial distance from inlet throat
Y	vertical distance from wall
y^+	law-of-the-wall coordinate, $u_\tau Y/\nu_w$
δ_{ef}	dimensionless engine face radius, $(R-R_s)/(R_{ef}-R_s)$
ν	kinematic viscosity
ρ	density
τ_w	wall shear stress

Subscripts:

ave	average
i	inlet throat
max	maximum
min	minimum

o free-stream condition

w wall

EXPERIMENTAL BACKGROUND

This section gives a brief description of the experiments that were conducted about 20 years ago at NASA Lewis by J.F. Wasserbauer, E.T. Meleason, and P.L. Burstadt ("Experimental Investigation of the Performance of a Mach-2.7 Two-Dimensional Bifurcated Duct Inlet with 30 Percent Internal Contraction," NASA Lewis Research Center, Cleveland, Ohio, 1970's, unpublished data.)

An experimental investigation was conducted to evaluate the performance of a two-dimensional, mixed-compression bifurcated inlet with 30 percent internal contraction. This inlet was designed for a free-stream Mach number of 2.7. The tests were conducted in the NASA Lewis Research Center's 10- by 10-Foot Supersonic Wind Tunnel over a Mach number range of 2.5 to 2.8 and a Reynolds number range of 2.5 to 2.3 million per foot. The free-stream total pressure Pt_o and total temperature Tt_o were 2500 lb/ft^2 and 680 R , respectively. Boundary layer bleed was located at the cowl, centerbody, and sidewalls. The experiments were conducted with and without vortex generators which were located on the cowl and centerbody of the subsonic diffusers. Vortex generators were very effective in redistributing the flow at the engine face; however, they were not effective in reducing distortion. An ejector bypass was located in the bypass door cavity. Approximately 2.5 percent of the duct airflow was bypassed in the experiments.

SOLUTION METHOD

The PARC code, originally developed at the Air Force Arnold Engineering Development Center, solves the full Reynolds-averaged Navier-Stokes equations in strong conservation form with the Beam and Warning approximate factorization. The code uses a central differencing scheme in a generalized curvilinear coordinate system with implicit and explicit second- and fourth-order artificial dissipation. The details of the code are found in reference 8.

The geometry of a single diffuser of the bifurcated inlet is shown in figure 2. The overall length of the diffuser is 36.98 in. The cross-sectional area of the diffuser changes from a rectangle (16.4 by 3.58 in.) to nearly a half circle. The transition of the cross-sectional area begins at X = 5.48 in. and ends at X = 35.48 in. A semispherical fairing (shown in fig. 2) starts at X = 28.8 in. and extends to the exit of the diffuser. The bypass cavity (shown in fig. 1) starts at X = 22.48, and ends at X = 28.73 in. The area ratio of the exit to entrance of the diffuser geometry is approximately 1.6. The area distribution of the diffuser geometry is shown in figure 2.

One-half of a single duct (one-quarter of the twin-diffuser system) was numerically simulated in the computations. The computational grid for this complex geometry (fig. 3) was generated using the GRIDGEN (ref. 9) grid generation program. The length of the computational domain was extended by one width (16.4 in.) of the diffuser to minimize the effect of the boundary condition applied at the exit. Of the 131 grid points used in the axial direction, 61 were uniformly distributed up to the start of the spinner fairing. A smaller grid spacing was used from the start of the fairing to the exit of the diffuser, with 50 grid points being uniformly distributed in this area. The remaining 20 grid points were uniformly distributed in the extended computational domain. A polar grid topology was chosen and consisted of 61 radial and 61 circumferential grid points. To resolve the viscous layer, the grid lines were packed close to the solid walls using hyperbolic tangent functions so that the first grid line was located at a $y+$ from 5 to 20 away from the walls. A total of 487 451 grid points were used.

The computations were performed for a throat Mach number of 0.74, obtained from previous experiments (J.F. Wasserbauer, E.T. Meleason, and P.L. Burstadt, "Experimental Investigation of the Performance of a Mach-2.7 Two-Dimensional Bifurcated Duct Inlet with 30 Percent Internal Contraction," NASA Lewis Research Center, Cleveland, Ohio, 1970's unpublished data.) The Reynolds number, based on the flow conditions at the subsonic diffuser entrance and inlet throat width D_i, was 4.47×10^6. In the computations, the inlet conditions at the duct entrance were assumed to be entirely subsonic, and a numerical simulation of the normal shock at the throat was not attempted. The diffuser inlet conditions obtained from the experiments were fixed. In the computations, an approximate average boundary layer profile was assumed from the available boundary layer data at the throat and was used

at the entrance of the diffuser. A no-slip adiabatic boundary condition was used on the solid surfaces. The boundary layer effect was taken into account when the nondimensional mass flow was calculated at the entrance of the diffuser. This nondimensional mass flow was used as the boundary condition at the exit of the computational domain. Anderson and Kapoor (ref. 7) found that the use of the mass flow boundary condition at the exit of the computational domain significantly improved the numerical results as compared with those when the pressure boundary condition was used. The nondimensional mass flow boundary condition was also used to simulate the bypass flow.

The Baldwin-Lomax (ref. 10) turbulence model used in this study is an algebraic eddy viscosity model. In the present computations, the Baldwin-Lomax turbulence model was modified to improve the simulation of reverse flow regions as suggested by Deiwert (ref. 11). In the region of reverse flow, the inner layer is replaced with the outer model which extends all the way to the wall. In the absence of reverse flow, the conventional Baldwin-Lomax turbulence model is used. This modification of the Baldwin-Lomax turbulence model worked very well for the complex flow fields found in the S-ducts (refs. 6 and 7).

Computations were performed with and without bypass flows. With bypass flow, approximately 2.5 percent of theduct mass flow was allowed to leave through the bypass. All computations were performed without vortex generators on the CRAY-YMP supercomputer at NASA Lewis. The code typically required 20 hr of CPU time to achieve global convergence.

RESULTS AND DISCUSSION

Figure 4 shows the Mach number distribution at six axial planes along the length of the subsonic diffuser. A few grid lines are also shown to represent the diffuser geometry. The Mach number at the entrance of the diffuser is 0.74 and gradually decreases along the length of the diffuser. The boundary layer thickness also increases along the length of the diffuser. As seen in figure 4, Mach numbers are reduced in the corners of the subsonic diffuser from axial plane 3 to the exit. The reduction in the Mach numbers in the corners becomes more prominent at axial planes 4 and 5. However, the Mach number increases slightly at the exit of the diffuser because the presence of the spinner fairing actually reduces the area distribution (as shown in fig. 3). The computations did not indicate any large region of streamwise separation.

Figure 5 shows the Mach number distribution at the engine face. Figure 6 presents the crossflow velocity distribution at the engine face. The vectors are color coded according to Mach numbers. As a result of transverse pressure gradients, the flow moves radially inward and rolls up to make strong vortical flow at the corners. The secondary flow is clearly shown.

Figure 7 shows the total pressure recovery at six axial planes. As seen in the figure, the total pressures remain almost constant in the central core of the flow, indicating that there are practically no losses in the core flow. However, there is a total pressure loss near the corner as a result of the vortical flows. The size of the vortex increases as it moves downstream along the length of the diffuser.

In experiments (J.F. Wasserbauer, E.T. Meleason, and P.L. Burstadt, "Experimental Investigation of the Performance of a Mach-2.7 Two-Dimensional Bifurcated Duct Inlet with 30 Percent Internal Contraction," NASA Lewis Research Center, Cleveland, Ohio, 1970's, unpublished data), the total pressure recovery at the engine face was measured by an eight-arm total pressure rake. The arms were located at 10°, 30°, 90°, 150°, 190°, 210°, 270°, and 330° measured counterclockwise from the horizontal. Nine total pressure probes were located on each arm. The experimental area weighted total pressure recovery was 0.9529.

The computed total pressure recovery distribution at the engine face, shown in figure 8, is almost 1.0 in the core flow but reduces to about 85 percent near the walls because of the thick boundary layer and in the corners because of vortical flows. To compare the computational total pressure recovery with experimental results, the numerical total pressures were calculated at the same locations as those of the total pressure probes in experiments. The computational total pressure recovery calculated based on the location of experimental probes is 0.9502. It is evident that the present computations show excellent agreement with experimental total pressure recovery.

Computational results with 2.5-percent bypass flow show the total pressure recovery as calculated in the previous paragraph to be 0.9630. This shows that the bypass flow actually increases the total pressure recovery at the engine face. Similar results were reported by Ball (ref. 12) and Lee and Boedicker (ref. 13), where a boundary layer bleed system was used to remove up to 5 percent of the diffuser entrance mass flow.

Figure 9 compares the surface ramp pressure distributions with experiment. The surface ramp pressures were measured at the centerline of the duct. In figure 9, the pressure is nondimensionized by the free-stream total

pressure Pt_o and the axial distance is nondimensionized by the inlet throat width D_i. The surface pressure on the ramp compares reasonably well with experimental data. The peak seen in the computational pressure at $X/D_i = 1.76$ is actually at the tip of the spinner fairing. As discussed earlier, the shape of the spinner fairing was semispherical, and in the computations, the grid resolution was not fine enough to accurately model the leading edge of the spinner fairing. This numerical error could be removed by providing a very fine grid resolution, but, to save CPU time, this was not attempted. Figure 10 compares the surface cowl pressure distributions with experiment. The surface pressures on the cowl compare reasonably well with experimental data.

The surface ramp and cowl pressures at the engine face are slightly overpredicted in the computations, which indicates that the computational and experimental mass flows were not exactly the same. The reason may be that the exact experimental mass flow could not be calculated because there were no detailed boundary profiles at the throat.

The calculated diffuser mass flow with and without bypass flow is shown in figure 11. The diffuser mass flow without bypass remains at almost 1.0 along the entire length of the diffuser. As expected, the diffuser mass flow was approximately 2.5 percent less at the location of the bypass openings, which indicates the accuracy of the bypass flow boundary conditions in the computations.

Figure 12 presents the average total pressure Pt_{ave} at the engine face. The effect of bypass flow is also shown in the figure. In the discussion of figure 9, the bypass flow improved the total pressure recovery at the engine face.

Figures 13 and 14 show the radial ring and 60° circumferential distortions at the engine face, respectively. The definitions of distortion parameters are the same as those used in reference 7. The radial ring distortion was relatively higher near the spinner fairing and cowl. This trend is consistent with the results obtained in reference 7. The effect of bypass flow on the radial ring distortion is very small. The 60° circumferential ring distortion (fig. 14) remains relatively uniform in the central portion of the engine face. The present calculations show that the bypass flow significantly reduces the circumferential distortion at the engine face.

CONCLUSIONS

The PARC3D code, which solves the three-dimensional Reynolds-averaged full Navier-Stokes equations with the Baldwin-Lomax turbulence model, was applied to the subsonic diffuser section of the NASA Lewis Research Center's 70/30 mixed-compression bifurcated supersonic inlet. Also computed was the case with approximately 2.5 percent bypass flow. The computational results were compared with the available experimental data.

The computations show the presence of strong vortical flows in the corner, affecting the total pressure recovery and flow distortion at the engine face. The total pressure recovery, Mach number, crossflow velocity, and flow distortions at the engine face were obtained. The surface ramp and cowl pressure distributions and the total pressure recovery at the engine face compared very well with experimental data. The CFD analysis demonstrated that the bypass flow improves the total pressure recovery and reduces flow distortions at the engine face.

ACKNOWLEDGMENTS

This research was conducted while the first author held a National Research Council Research Associateship at NASA Lewis Research Center. The authors are grateful to Mr. Joseph F. Wasserbauer of NASA Lewis Research Center for providing the geometry and experimental results of the bifurcated inlet. The authors greatly appreciated the assistance of Dr. Danny P. Hwang (of NASA Lewis) who generated the grid of the diffuser geometry.

REFERENCES

1. Briley, W.R.; and McDonald, H.: Analysis and Computation of Viscous Subsonic Primary and Secondary Flow. AIAA Paper 79–1453, 1979.
2. Briley, W.R.; and McDonald, H.: Three-Dimensional Viscous Flows with Large Secondary Velocities. Fluid Mech., vol. 144, Mar. 1984, pp. 47–77.

3. Anderson, B.H.: The Aerodynamic Characteristics of Vortex Ingestion for the F/A-18 Inlet Duct. AIAA Paper 91–0130, 1990.
4. Harloff, G.J.; Reichert, B.A.; and Wellborn, S.R.: Navier-Stokes Analysis and Experimental Data Comparison of Compressible Flow in Diffusing S-Duct. AIAA Paper 92–2699, 1992.
5. Sirbaugh, J.R.; and Reichert, B.A.: Computation of the Circular-to-Rectangular Transition Duct Flow Field. AIAA Paper 91–1741, 1991.
6. Anderson, B.H.; Reddy, D.R.; and Kapoor, K.: A Comparative Study of Full Navier-Stokes and Reduced Navier-Stokes Analyses for Separating Flows Within a Diffusing Inlet S-Ducts. AIAA Paper 93–2154, 1993.
7. Anderson, B.H.; and Kapoor, K.: A Study on Bifurcated Transitioning S-Ducts for High-Speed Inlet Application, AIAA Paper 94–2812, 1994.
8. Cooper, G.K.: The PARC Codes. Report AEDC–TR–87–24, Arnold Engineering Development Center, Tullahoma, TN, Oct. 1987.
9. Steinbrenner, J.P.; Chawner, J.P.; and Fouts, C.L.: The GRIDGEN3D Multiple Block Grid Generation System. Users' Manual, Report WRDC–TR–90–3022, vol. II, July 1990.
10. Baldwin, B.; and Lomax, H.: Thin-Layer Approximation and Algebraic Model for Separated Turbulent Flows. AIAA Paper 78–257, 1978.
11. Deiwert, G.S.: Computation of Separated Transonic Turbulent Flows. AIAA J., vol. 14, no. 6, June 1976, pp. 735–740.
12. Ball, W.M.: Experimental Investigation of Effects of Wall Suction and Blowing on the Performance of Highly Offset Diffusers. AIAA Paper 83–1169, 1983.
13. Lee, C.C.; and Boedicker, C.: Subsonic Diffuser Design and Performance for Advanced Fighter Aircraft. AIAA Paper 85–3073, 1985.

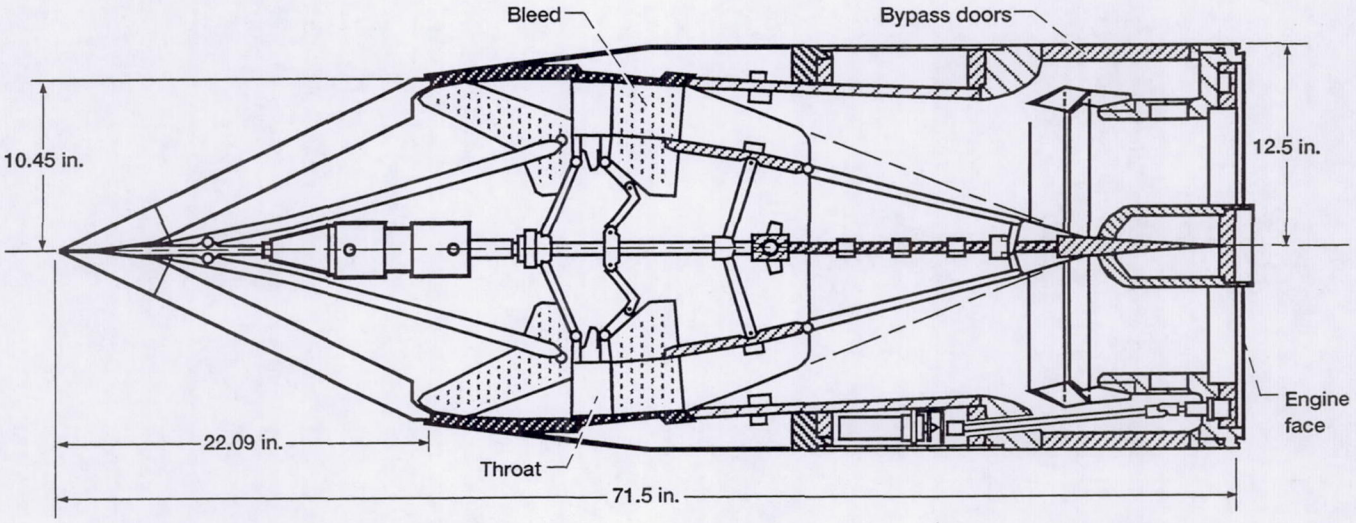

Figure 1.—The NASA Lewis Research Center's 70/30 mixed-compression bifurcated supersonic inlet. Inlet width, 16.4 in.

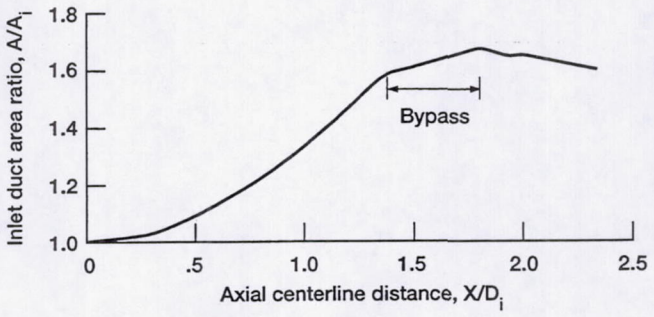

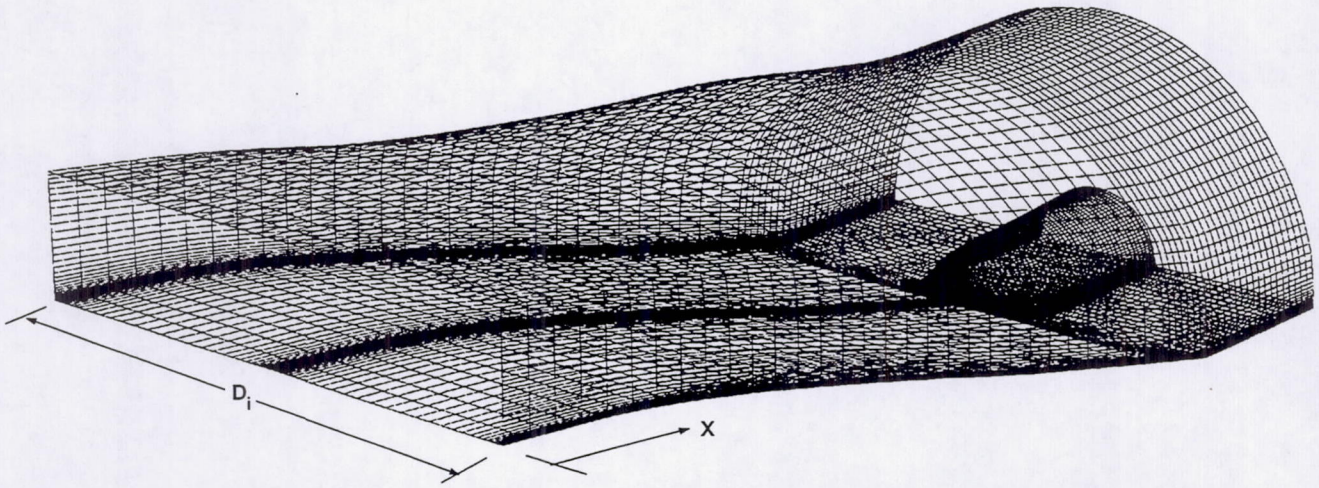

Figure 2.—Geometry and area distribution of subsonic diffuse of bifurcated supersonic inlet.

Page Intentionally Left Blank

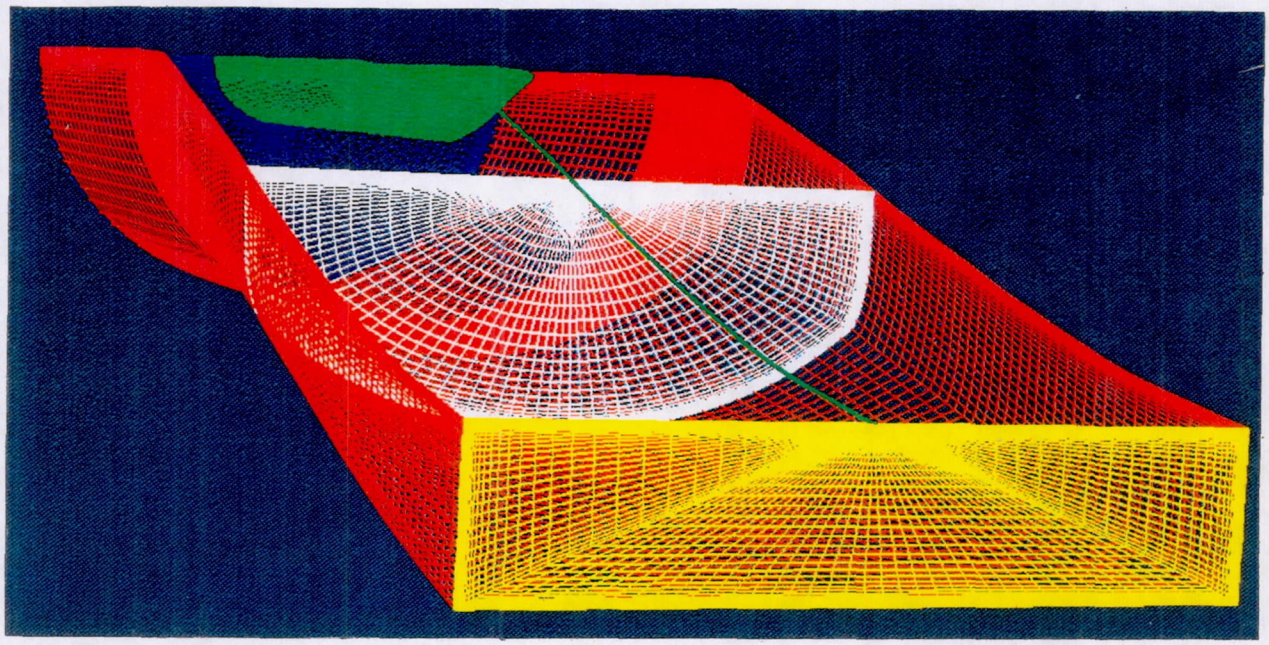

Figure 3.—Computational grid generated for diffuser geometry. Grid size, 131 by 61 by 61.

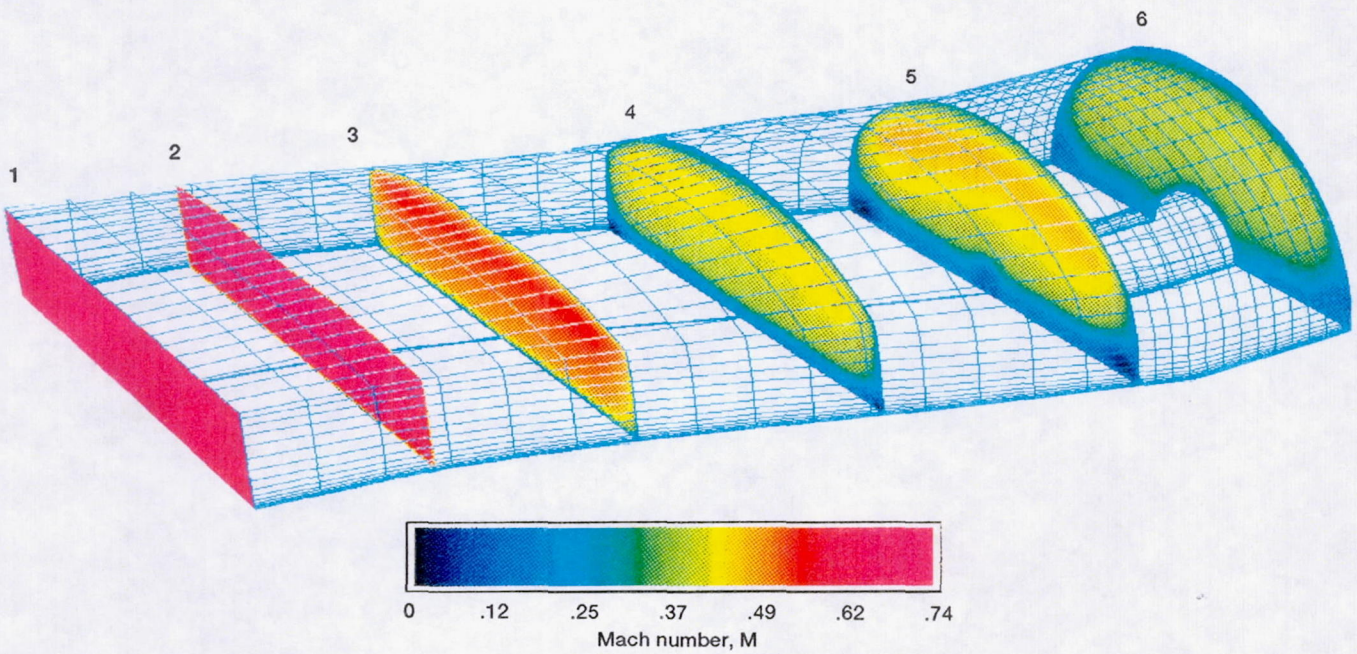

Figure 4.—Mach number distribution along length of subsonic diffuser.

Page Intentionally Left Blank

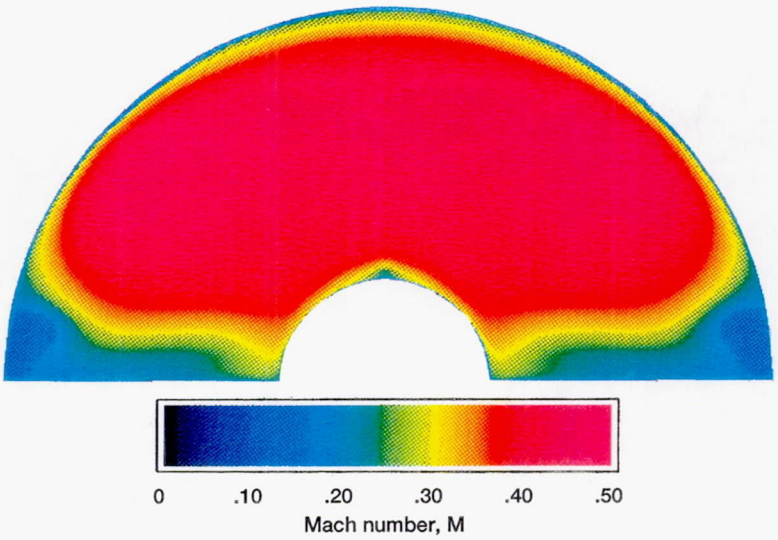

Figure 5.—Mach number distribution at engine face.

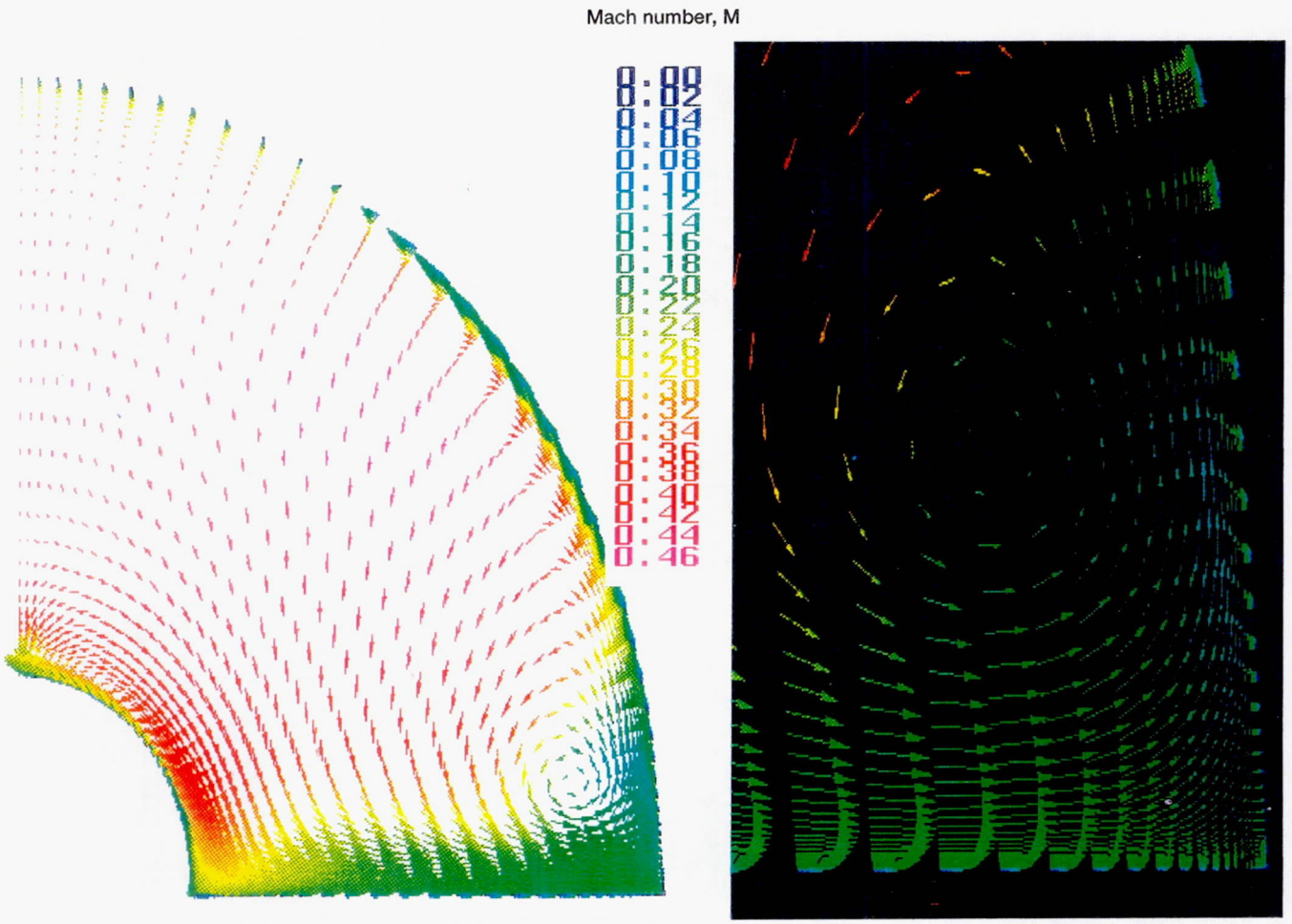

Figure 6.—Crossflow velocity (color-coded by Mach number) at engine face.

Page Intentionally Left Blank

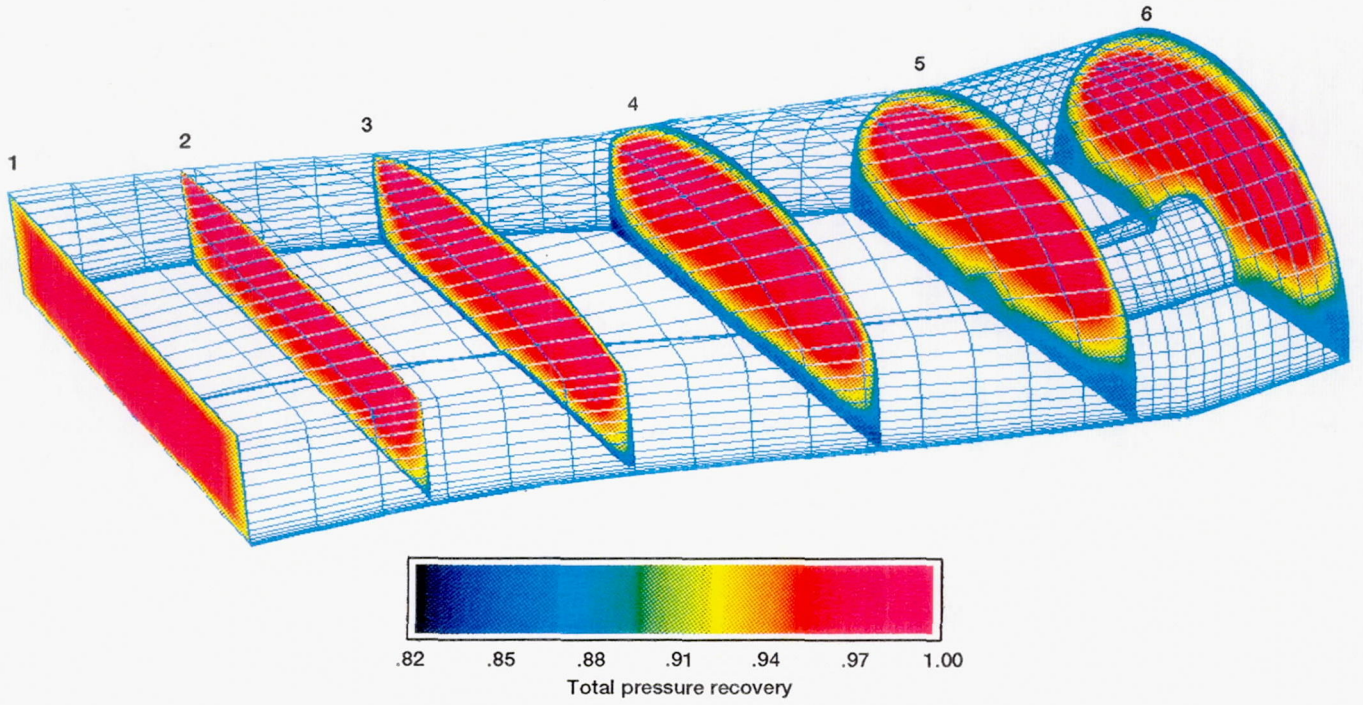

Figure 7.—Total pressure recovery along length of subsonic diffuser.

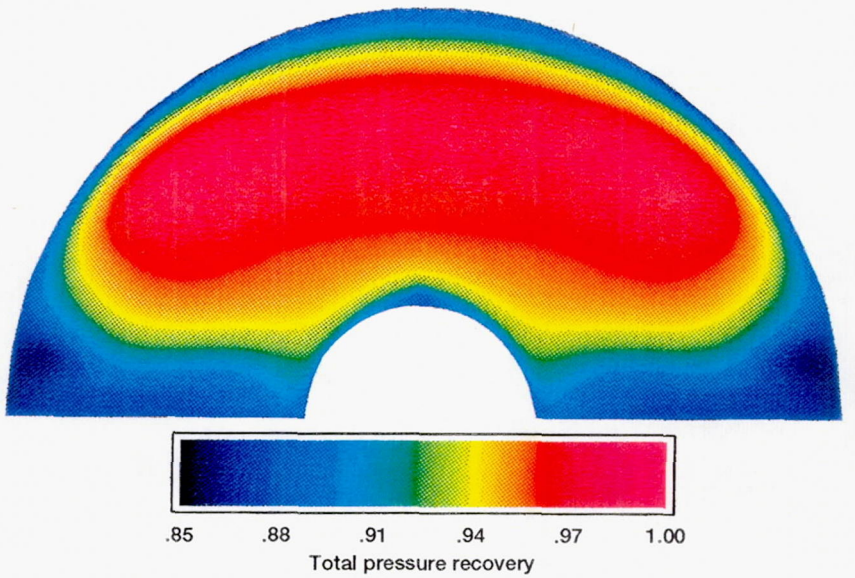

Figure 8.—Total pressure recovery at engine face.

Page Intentionally Left Blank

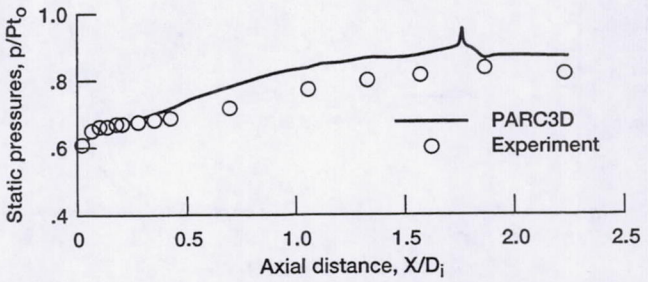

Figure 9.—Comparison of surface ramp pressure distribution with experiment.

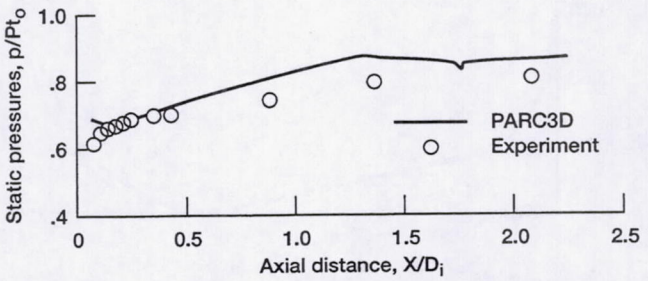

Figure 10.—Comparison of surface cowl pressure distribution with experiment.

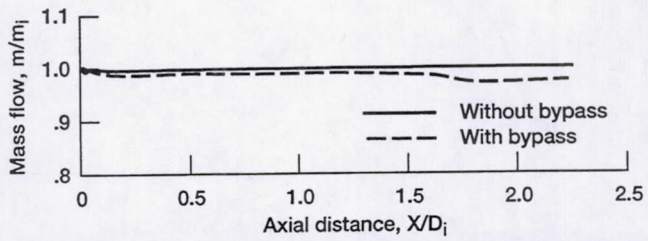

Figure 11.—Calculated mass flow along length of subsonic diffuser.

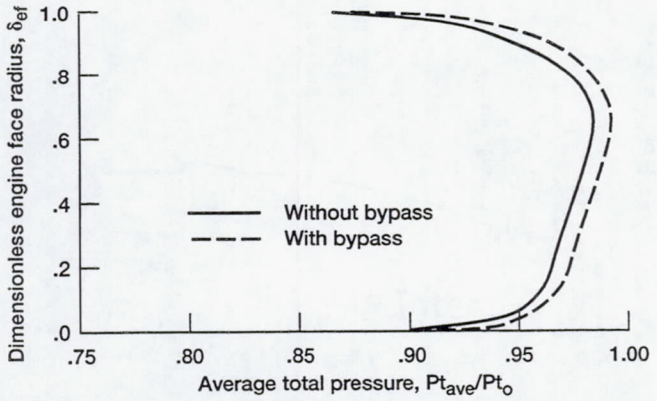

Figure 12.—Effect of bypass flow on total pressure distribution at engine face.

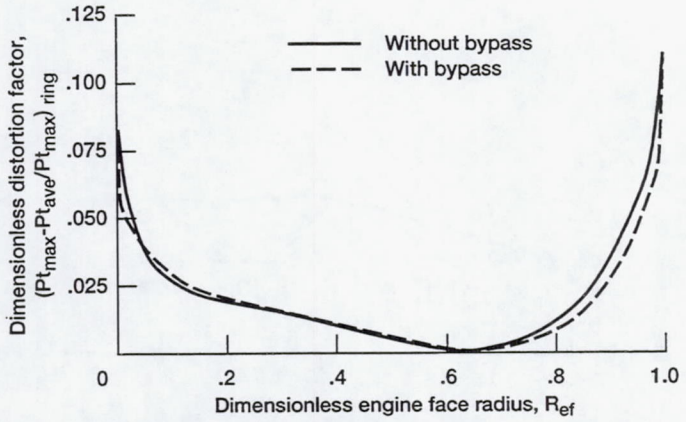

Figure 13.—Calculated radial ring distortion at engine face.

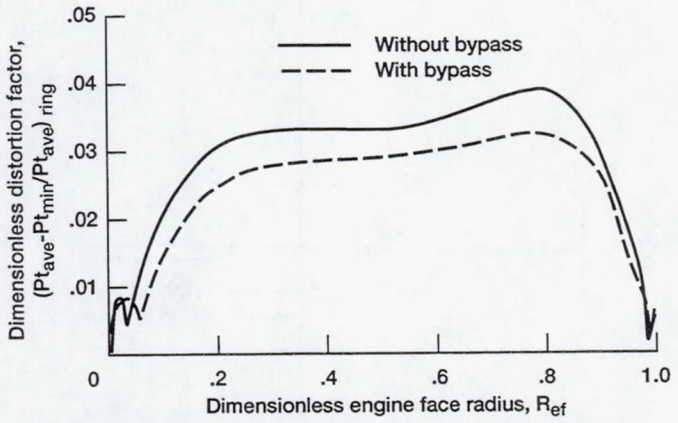

Figure 14.—Calculated 60° sector circumferential distortion at engine face.

REPORT DOCUMENTATION PAGE

Form Approved
OMB No. 0704-0188

1. AGENCY USE ONLY (Leave blank)	2. REPORT DATE	3. REPORT TYPE AND DATES COVERED
	July 1994	Technical Memorandum

4. TITLE AND SUBTITLE

A Full Navier-Stokes Analysis of Subsonic Diffuser of a Bifurcated 70/30 Supersonic Inlet for High Speed Civil Transport Application

5. FUNDING NUMBERS

WU-537-02-23

6. AUTHOR(S)

Kamlesh Kapoor, Bernhard H. Anderson, and Robert J. Shaw

7. PERFORMING ORGANIZATION NAME(S) AND ADDRESS(ES)

National Aeronautics and Space Administration
Lewis Research Center
Cleveland, Ohio 44135-3191

8. PERFORMING ORGANIZATION REPORT NUMBER

E-8939

9. SPONSORING/MONITORING AGENCY NAME(S) AND ADDRESS(ES)

National Aeronautics and Space Administration
Washington, D.C. 20546-0001

10. SPONSORING/MONITORING AGENCY REPORT NUMBER

NASA TM-106637

11. SUPPLEMENTARY NOTES

Responsible person, Thomas J. Biesiadny, organization code 2780, (216) 433-3967.

12a. DISTRIBUTION/AVAILABILITY STATEMENT

Unclassified - Unlimited
Subject Category 02

12b. DISTRIBUTION CODE

13. ABSTRACT ***(Maximum 200 words)***

A full Navier-Stokes analysis was performed to evaluate the performance of the subsonic diffuser of a NASA Lewis Research Center 70/30 mixed-compression bifurcated supersonic inlet for high speed civil transport application. The PARC3D code was used in the present study. The computations were also performed when approximately 2.5 percent of the engine mass flow was allowed to bypass through the engine bypass doors. The computational results were compared with the available experimental data which consisted of detailed Mach number and total pressure distributions along the entire length of the subsonic diffuser. The total pressure recovery, flow distortion, and crossflow velocity at the engine face were also calculated. The computed surface ramp and cowl pressure distributions were compared with experiments. Overall, the computational results compared well with experimental data. The present CFD analysis demonstrated that the bypass flow improves the total pressure recovery and lessens flow distortions at the engine face.

14. SUBJECT TERMS	15. NUMBER OF PAGES
Subsonic diffusers; Transitioning S-Duct; Bifurcated supersonic inlet diffuser; CFD analysis of diffusers	18
	16. PRICE CODE: A03

17. SECURITY CLASSIFICATION OF REPORT	18. SECURITY CLASSIFICATION OF THIS PAGE	19. SECURITY CLASSIFICATION OF ABSTRACT	20. LIMITATION OF ABSTRACT
Unclassified	Unclassified	Unclassified	